NeuroImage 225 (2021) 117458

Contents lists available at ScienceDirect

NeuroImage

journal homepage: www.elsevier.com/locate/neuroimage

Predicting brain age with complex networks: From adolescence to adulthood

Loredana Bellantuono[c,1], Luca Marzano[c,1], Marianna La Rocca[d], Dominique Duncan[d], Angela Lombardi[b], Tommaso Maggipinto[c], Alfonso Monaco[b,*], Sabina Tangaro[b,e], Nicola Amoroso[a,b,2], Roberto Bellotti[b,c,2]

[a] Dipartimento di Farmacia - Scienze del Farmaco, Universitá degli Studi di Bari Aldo Moro, Bari, Italy
[b] Istituto Nazionale di Fisica Nucleare, Sez. di Bari, Bari, Italy
[c] Dipartimento Interateneo di Fisica, Universitá degli Studi di Bari Aldo Moro, Bari, Italy
[d] University of Southern California, Laboratory of NeuroImaging, USC Stevens Neuroimaging and Informatics Institute, Keck School of Medicine of USC, Los Angeles, CA, United States
[e] Dipartimento di Scienze del Suolo, della Pianta e degli Alimenti, Universitá degli Studi di Bari Aldo Moro, Bari, Italy

ARTICLE INFO

Keywords:
Age prediction
Brain
Deep learning
MRI
Complex networks
ABIDE
Centrality measures

ABSTRACT

In recent years, several studies have demonstrated that machine learning and deep learning systems can be very useful to accurately predict brain age. In this work, we propose a novel approach based on complex networks using 1016 T1-weighted MRI brain scans (in the age range 7 – 64years). We introduce a structural connectivity model of the human brain: MRI scans are divided in rectangular boxes and Pearson's correlation is measured among them in order to obtain a complex network model. Brain connectivity is then characterized through few and easy-to-interpret centrality measures; finally, brain age is predicted by feeding a compact deep neural network. The proposed approach is accurate, robust and computationally efficient, despite the large and heterogeneous dataset used. Age prediction accuracy, in terms of correlation between predicted and actual age $r = 0.89$and Mean Absolute Error MAE = 2.19years, compares favorably with results from state-of-the-art approaches. On an independent test set including 262 subjects, whose scans were acquired with different scanners and protocols we found MAE = 2.52. The only imaging analysis steps required in the proposed framework are brain extraction and linear registration, hence robust results are obtained with a low computational cost. In addition, the network model provides a novel insight on aging patterns within the brain and specific information about anatomical districts displaying relevant changes with aging.

1. Introduction

Brain aging is a continuous and lifelong process. Although abnormal alterations must be carefully distinguished from physiological changes, it is manifest that general comorbidity factors and several pathologies, such as HIV (Zahr, 2018), schizophrenia (Schnack et al., 2016) and diabetes (Roriz-Filho et al., 2009), are well correlated with aging, not to mention neurodegenerative diseases, such as Alzheimer's disease, (Cole and Franke, 2017; Cole et al., 2018; Franke et al., 2010). Accordingly, the design and development of accurate age prediction models measuring "brain gap" (Franke and Gaser, 2019), i.e. the difference between the predicted brain age and the actual one, are crucial to help identifying novel markers for such diseases and provide sound systems for early diagnosis.

In recent years, machine learning and deep learning approaches have demonstrated the possibility to accurately predict age from brain MRI scans (Aycheh et al., 2018; Madan and Kensinger, 2018). Two different strategies have been typically adopted: the preferred one consists of extracting a compact representation of data, usually exploiting a combination of various pre-processing, feature extraction and supervised learning techniques (Ashburner, 2007; Erus et al., 2015; Konukoglu et al., 2013; Sabuncu and Van Leemput, 2012); an alternative approach, exploiting raw high-dimensional data, is currently attracting significant interest, especially thanks to novel advances provided by convolutional neural networks (Cole et al., 2017; Feng et al., 2020; Putin et al., 2016). Exhaustive reviews of the field have been recently published (Cole et al., 2019; Franke et al., 2017). In the present work, we propose a novel approach to age prediction based on graph theory.

* Corresponding author.
E-mail address: alfonso.monaco@ba.infn.it (A. Monaco).
[1] Equal first author contribution.
[2] Equal last author contribution.

https://doi.org/10.1016/j.neuroimage.2020.117458
Received 14 September 2020; Accepted 13 October 2020
Available online 21 October 2020

Regarding neuroimaging, brain connectivity has been extensively studied from both functional and structural perspectives. Starting from functional MRI data, it is possible to measure synchronization of different anatomical regions and use mathematical pairwise similarity measurements to construct a network model. This kind of approach has been suitably adopted in several contexts, ranging from schizophrenia to autism and aging, too (Abellaneda-Pérez et al., 2019; Bagarinao et al., 2019; Lombardi et al., 2019; Spreng et al., 2016). Concerning structural connectivity, the situation is more variegated. Initial approaches to structural brain connectivity relied on segmentation of brain regions and measurements of volume covariance; this panorama substantially changed with diffusion data, for which several algorithms allow the evaluation of physical connections (Damoiseaux, 2017; Fjell and Walhovd, 2010; Wu et al., 2020).

In graph theory, a complex network is a collection of interconnected objects, which can be represented in visual and mathematical terms with a diagram, called a graph. The elements of the complex network are referred to as nodes or vertices, and their mutual connections are called links or edges. A network yields an overall description of the system under investigation, e.g. unveiling the dynamics that determines its organization; besides, specific network properties known as centrality measures characterize the importance of each node, by taking into account the number and quality of its connections. In the following, we shall assume that aging processes affect the local organization of the brain and, therefore, that network centralities can be a reliable proxy of aging. This hypothesis is motivated by our previous works, where we explored multiplex network models for the early diagnosis of brain diseases (Amoroso et al., 2019; 2018a; 2018b; La Rocca et al., 2018). In particular, studying Alzheimer's disease and Parkinson's disease, we observed how a multiplex network could accurately model neurodegenerative patterns. However, this work presents some fundamental differences from the previous ones: first of all, the model proposed here is mathematically simpler, as it is based on single subject networks instead of multiplex ones; moreover, it is easier to interpret because it exploits only features directly related to nodes and therefore concerning a specific anatomical counterpart; finally, it is more efficient from the computational perspective.

As far as we know, the results presented here are the most accurate ones achieved for age prediction with a complex network model. In general, we demonstrate that a network model can be profitably used to shed light on the mechanisms that relate brain connectivity and aging and, above all, to characterize these mechanisms from an anatomical perspective. This result is remarkable compared with other studies, in which an intuitive interpretation is often hindered by model complexity. Finally, it is worth mentioning that our results were achieved on the Autism Brain Imaging Data Exchange I (ABIDE I) dataset, which is particularly challenging to analyze because of its heterogeneity, due for example to the number of different data collection sites and acquisition protocols.

2. Materials

Data examined in this work were collected by the ABIDE initiative from 17 different international sites, and refer to various acquisition protocols (Di Martino et al., 2014). These data include $T1-$weighted MRI brain scans of 1112 individuals, whose age ranges from 7 to 64 years, with a mean value of 17 ± 8years, which makes the data distribution highly right-skewed; for each scan, the age of patients is provided, see Table 1 for a synthetic per-site overview.
[3]

Table 1
Enrolled subjects, age range and clinical diagnosis of ABIDE I dataset per site. The list of acronyms is reported in footnote[4].

Site	Enrolled	Age (yr)	(NC/ASD)
CAL	38	17–56	19/19
CMU	27	19–40	13/14
KKI	55	8–12	33/22
LEU	64	12–32	35/29
MUN	57	7–58	33/24
NYU	184	7–39	105/79
OHSU	28	8–15	15/13
OLIN	36	10–24	16/20
PITT	57	9–35	27/30
SBL	30	20–64	15/15
SDSU	36	8–17	22/14
STAN	40	7–12	20/20
TRI	49	12–26	25/24
UCLA	109	9–18	47/62
UM	145	8–29	77/68
USM	101	9–50	43/58
YALE	56	7–18	28/28

The subjects can be divided into two clinical cohorts: patients affected by Autism Spectrum Disorder (ASD) and age-matched normal controls (NC). Some useful information provided by ABIDE initiative is a quality rating assigned by three human experts to every MRI scan. The rating has three possible labels: "Ok", "maybe" or "fail"; in some cases, notes explaining the judgment are present too. Although all images considered in this work are collected with 3 Tesla scanners, data are extremely heterogeneous: scanners from different manufacturers were used, and even in the rare circumstances in which the same scanner was employed, echo time, repetition time, flip angle and field of view (just to mention a few typical MRI parameters) were set with different values. A detailed description of scan procedures and MRI parameters by site are available at http://fcon_1000.projects.nitrc.org/indi/abide ; it is worth mentioning that data used in this paper are also publicly available, on the same site, and free to download after registration.

Considering the heavy right-skewness of age distribution, 22 subjects older than 40 years were excluded from this study; moreover, we disregarded 29 subjects whose quality rating included 2 "fail" marks and 45 subjects whose MRI data were affected by registration errors, thus resulting in a final set of 1016 subjects with mean age 16 ± 6years, representing $91\%$of the entire database. An independent and heterogeneous test set was performed, using 262 subjects in the age range 7–40 years: 78 subjects from ABIDE I and 184 subjects from Beijing Normal University[4] database were uniformly sampled according to the age distribution.

3. Methods

3.1. Overview of methodology

The overview of the proposed approach is illustrated in Fig. 1. The method consists of two main phases: network modeling and learning.

In the modeling phase, each MRI brain scan undergoes a fully automated processing pipeline aiming at correcting gray-level inhomogeneities, due to magnetic field bias, and spatial normalization. Scans were skull-stripped with the Brain Extraction Tool (Jenkinson et al., 2005) and inhomogeneity-corrected with the N4 algorithm (Tustison et al., 2010). Then, all images and brain volumes

[3] California Institute of Technology (CAL), Carnegie Mellon University (CMU), Kennedy Krieger Institute (KKI), Univeristy of LEUVEN (LEU), Ludwig Maximilians University Munich (MUN), NYU Langone Medical Center (NYU), Oregon Health and Science University (OSHU), Olin Institute of Living at Hartford Hospital (OLIN), University of Pittsburgh School of Medicine (PITT), Social Brain Lab BCN NIC UMC Groningen and Netherlands Institute for Neurosciences (SBL), San Diego State University (SDSU), Stanford University (STAN), Trinity Centre for Health Sciences (TRI), University of California Los Angeles (UCLA), University of Michigan (UM), University of Utah School of Medicine (USM), Yale Child Study Center (YALE).

[4] http://fcon_1000.projects.nitrc.org/indi/retro/BeijingEnhanced.html .

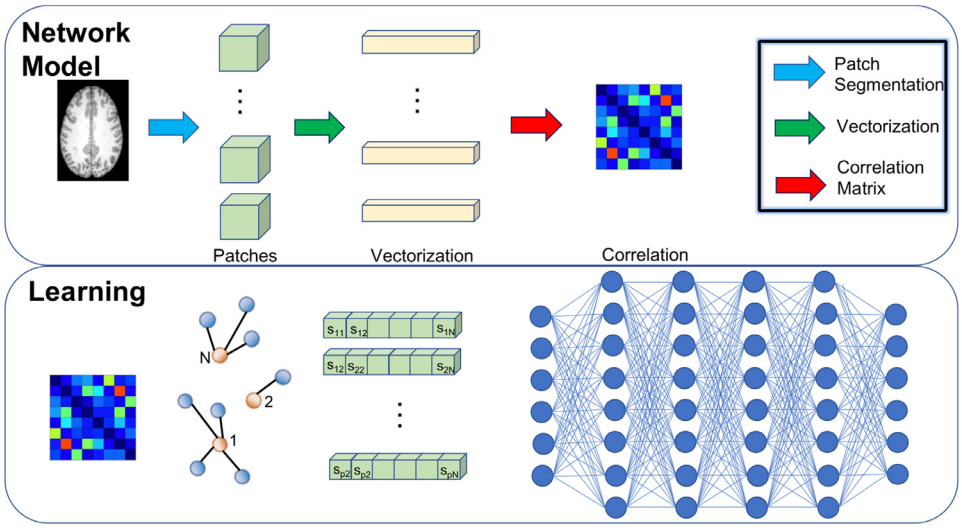

Fig. 1. The proposed method is divided in two phases: network modeling and learning. After MRI data is co-registered, patches are extracted and vectorized, then a correlation matrix is computed. The nodal strength is computed for all nodes, and this feature representation feeds a deep neural network.

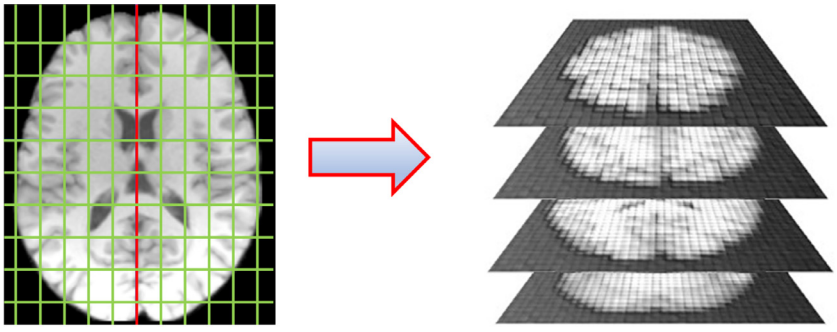

Fig. 2. After spatial normalization, each MRI scan is divided in homologous rectangular boxes called patches.

were spatially normalized with a linear affine registration (Avants et al., 2011) to the MNI152 reference space, with dimensions $182 \times 218 \times 182$and $1 \times 1 \times 1\text{mm}^3$resolution.

We deliberately decided not to include in such a pipeline any step that was not strictly necessary to achieve a robust standardization. Non-linear registration, artifact removal and signal-to-noise ratio enhancement are just a few examples of possible neuroimaging analyses which have been avoided here. Actually, we preferred to ensure a sub-optimal correspondence of gray-level distributions and anatomical regions, keeping the analysis free from compelling computational requirements and debates about the adoption of the optimal cutting-edge technique, provided that within the neuroimaging community, the choice of a particular software or a specific imaging pipeline has not gained a consensus yet.

After spatial normalization, we segmented the brain into Nrectangular boxes, called patches; the patches in which non-brain voxels represent more than 10%of the patch volume were not considered in the analysis. Interestingly, the patch size has a negligible effect on the model accuracy over a wide range of patch volumes (< 2500voxels). Further details about the patch segmentation and their dimensions (p_1, p_2, p_3) are discussed in the Supplementary materials (section Machine Learning Strategies).

Thus, each MRI scan is represented by a collection $\mathcal{N} = \{1, ..., N\}$of patches, see Fig. 2.

Then, it is straightforward to introduce the network model by considering the set of all the $n = N \cdot (N-1)/2$patch pairwise similarities $\mathcal{L} = \{l_1, l_2, ..., l_n\}$,measured between each pair of patches using Pearson's correlation. The couple $(\mathcal{N}, \mathcal{L})$defines a mathematical object called a graph, i.e. our complex network.

3.2. Network modeling

For a complex network $G = (\mathcal{N}, \mathcal{L})$,$\mathcal{N}$represents the set of nodes and $\mathcal{L}$the set of links. The nodes are the elements of interest within the system to study while the links represent their mutual interactions. In general, there is not a unique recipe to identify nodes and connections of a system; on the contrary, it is up to investigators to conceive the most suitable model for a specific situation. For neuroimaging, several network models have been already proposed (Betzel and Bassett, 2017; Bullmore and Sporns, 2009; Cannistraci et al., 2013; Qi et al., 2019; Zhou et al., 2006): functional or structural imaging, cross-sectional or longitudinal data, single-subject or group-wise models are just a few examples of the diversified strategies employed so far.

Using the previously mentioned patches, we defined our own brain network. A patch includes a fixed number of voxels, whose gray levels may be seen as components of a vector. To measure the pairwise similarity between two patches, we used Pearson's correlation; to take into account symmetrical parity, only absolute correlations were used. Using correlations is motivated by three reasons: (i) correlations take into account both the similarity of gray-level distributions within a patch and their spatial configuration; (ii) they are fast to compute and easy to implement, thus not involving any computational drawback; (iii) correlations have a straightforward interpretation, making them a good choice for clinical purposes.

The proposed model depends on three free parameters that cannot be determined *a priori* and require an accurate evaluation: the patch dimensions (p_1),$(p_2)$and (p_3),which are taken along the perpendicular directions to the coronal, the axial and the sagittal planes, respectively. Once these dimensions are set, the overall number of nodes within the network is defined by the need to cover the whole brain. For the present study, we used a $p_1 = 15$mm, $p_2 = 10$mm and $p_3 = 10$mm configuration,

resulting in a network with $N = 1184$nodes. Measuring pairwise similarities, we obtained a complete graph, i.e. a network whose nodes are maximally connected to each other. Such a network is particularly challenging to manage, as it has $N(N-1)/2$connections, which for the present case account for $\sim 10^6$elements. As suggested by Mukaka (2012), we set to zero the correlations below the 0.3 value as they are considered *negligible*. Accordingly, we applied a threshold to connections and set to zero those ones with correlation below 0.3, on average $\sim 10^4$spurious connections.

Finally, it is worth mentioning that each patch can contain several anatomical regions so we can consider the network neither strictly anatomical nor functional. However, since our model has been developed starting from $T1$-weighted images, we can regard it as falling within the large domain of structural connectivity.

3.3. Learning

The second phase of our framework is dedicated to learning from the network model. As the goal of our study is to capture brain changes due to aging effects, it is reasonable to assume that the main features detecting such changes should be those related to nodal centrality. Besides, it is worth to observe that, for clinical interpretability, it is desirable to deal with properties which can easily be related to brain anatomy.

In general, three distinct types of centrality measures are distinguished: metrics like strength evaluate the direct influence a node has on the others; if we are interested in the mediative effect of a node, in these situations a proper centrality measure is betweenness; when it is desirable to consider centrality from a global perspective, measures like eigenvector centrality are preferred, see Network Centralities in Supplementary Materials for formal definitions. Based on these considerations, we opted for nodal strength. This network centrality measure is used to evaluate the nodal importance and the direct effects a node has onto its neighbors.

Accordingly, we obtained an $S \times N$tabular representation of our data, where $S$is the number of subjects; then, we fed a deep neural network to extract and shape non-linear patterns eventually relating network centralities and aging. Our hypothesis was that a deep neural network would be an appropriate option to manage the intrinsic complexity of the brain and identify features which accurately predict its age. Recent studies have demonstrated the effectiveness of deep learning approaches for MRI analyses within a large number of different domains and several purposes (Benou et al., 2017; Durstewitz et al., 2019; Leibig et al., 2017).

Our proposed architecture is a feedforward deep neural network implemented with the "h2o" R package.[5] Whenever possible, we used the default values in order to avoid overfitting issues and emphasize the robustness of our connectivity model. The hyper-parameters explored with a grid-search approach were the number of hidden layers, the number of neurons and the activation functions. By default, h2o implements an adaptive learning rate for its stochastic gradient descent optimization. This algorithm depends on two parameters, $\tau$and ϵ,which control the balance of global and local search efficiencies; $\tau$is the similarity to prior weight updates and $\epsilon$is a parameter preventing the learning to be stopped in a local minimum. Defaults values $\tau = 0.99$and $\epsilon = 10^{-8}$were used. In training, we determined our best configuration consisting of four hidden layers with 200, 100, 50, and 20 neurons, respectively. The activation functions leading to the best performance for both accuracy and computational burden was the linear rectifier. The tuning of the parameters was set according to the performances obtained on a fraction of training examples that were used for internal validation.

To evaluate the performance of our model, we used three distinct metrics: Mean Absolute Error (MAE), Root Mean Squared Error (RMSE) and Pearson's correlation (ρ). All performed analyses employed 100 repeated 10−fold cross-validations to assess robustness and generalization power in the regression task. Finally, as there is no *a priori*reason to prefer deep neural networks over state-of-the-art regressors (Ho and Pepyne, 2002), we also employed Random Forest (Liaw et al., 2002), Lasso regression (Tibshirani, 1996), Ridge regression (Hoerl, 1986), Elastic Net (Zou and Hastie, 2005), Support Vector Machine (Smola and Schölkopf, 2004) and Relevance Vector Machine (Tipping, 2000); further details on their prediction accuracies are discussed in the Supplementary Materials (Section Machine Learning Strategies).

[5] https://www.h2o.ai/

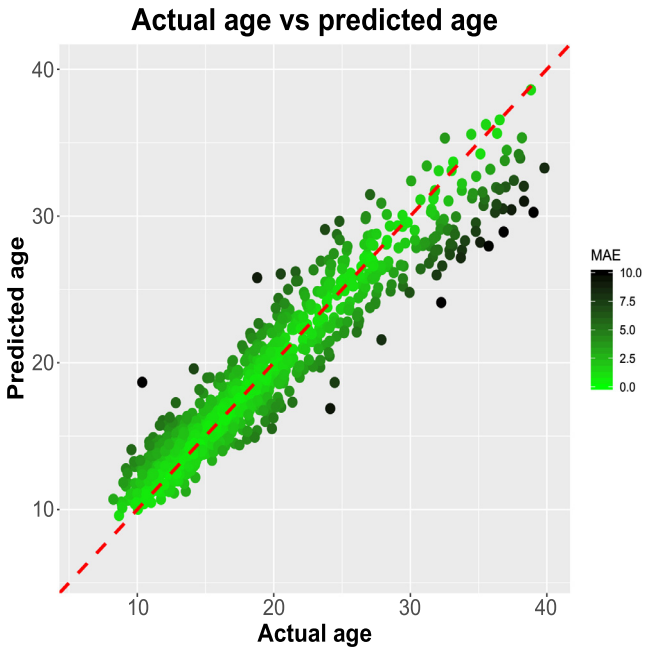

Fig. 3. Age predicted according to network model compared with actual age of each subject.

Table 2
For each algorithm we report mean and standard deviation of Mean Absolute Error (MAE), Root Mean Squared Error (RMSE) and Pearson's correlation ρ. Results are obtained with 100 10−fold cross-validation rounds.

Algorithm	MAE	RMSE	ρ
Deep learning	**2.19 ± 0.02**	**2.91 ± 0.03**	**0.890 ± 0.003**
Random Forests	3.09 ± 0.02	4.13 ± 0.03	0.770 ± 0.006
Lasso	2.54 ± 0.02	3.34 ± 0.02	0.850 ± 0.002
Ridge	2.49 ± 0.01	3.29 ± 0.02	0.858 ± 0.002
Elastic net	2.50 ± 0.02	3.30 ± 0.02	0.855 ± 0.002
Support Vector Machine	2.40 ± 0.03	3.19 ± 0.04	0.870 ± 0.004
Relevance Vector Machine	2.48 ± 0.03	3.25 ± 0.03	0.859 ± 0.003

4. Results

4.1. Age prediction: accuracy and robustness

Analysis showed that our complex network model allows robust age predictions despite using several different learning algorithms. Best performance is achieved using a deep neural network, see Fig. 3.

Prediction accuracy in terms of MAE and RMSE is 2.19 ± 0.03years and 2.91 ± 0.03,respectively; in terms of Pearson's correlation $\rho = 0.890 \pm 0.003$. The comparison with other learning methods is presented in Table 2.

Although all methods show accurate predictions in terms of all three metrics, deep neural network is significantly better ($p < 10^{-4}$after Bonferroni correction). Random Forest regression is the least accurate with MAE $= 3.09 \pm 0.02$,RMSE $= 4.13 \pm 0.03$and $\rho = 0.770 \pm 0.004$. The MAE

Table 3
Comparison between training and test performance.

Dataset	MAE	RMSE	ρ
Training	2.19 ± 0.02	2.91 ± 0.03	0.890 ± 0.003
Test	2.5 ± 0.2	3.2 ± 0.2	0.78 ± 0.02

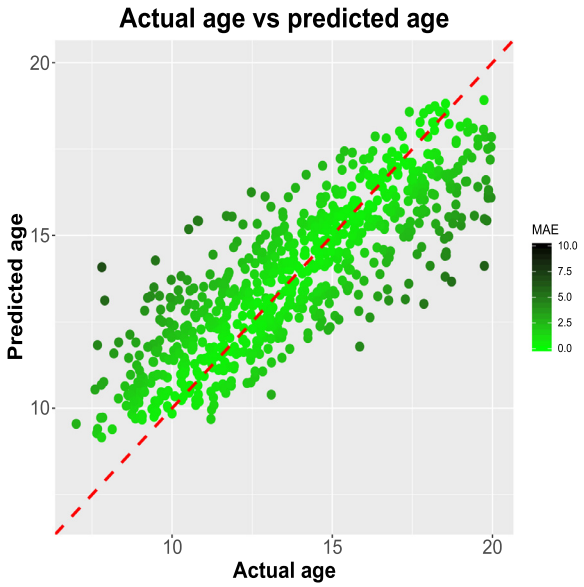

Fig. 4. Age prediction and actual age comparison for subjects of age 7–20 years.

provides a direct way to assess the differences among the various learning methods; in fact, the difference from the best performing algorithm and the worst one is just 1.04 years, corresponding to a relative uncertainty of about 3%.

4.2. Generalization on an independent test set

To evaluate how the results of the proposed connectivity model generalize when considering independent data, possibly acquired with different scanners and protocols, we ran the model learnt using the training set on an independent test set of 262 subjects whose age ranged from 7 to 40 years.

The cross-validation models trained with only ABIDE data were then used for prediction. In this way, we were able to estimate not only the performance metrics but also their uncertainties. Results are reported in the following Table 3 along with training metrics for comparison.

A statistically significant deterioration was detected in all reported metrics, especially when considering correlation. As a final remark, it is worth noting that test uncertainties, in terms of standard deviations, are larger by an order of magnitude than those obtained in training.

For further comparison, we investigated the test perfomance by dividing ABIDE and Beijing subjects, in fact we found for ABIDE subjects MAE $= 2.3 \pm 0.3$,RMSE $= 3.0 \pm 0.3$and $\rho = 0.40 \pm 0.04$while for Beijing subjects MAE $= 2.7 \pm 0.2$,RMSE $= 3.7 \pm 0.2$and $\rho = 0.85 \pm 0.03$.

4.3. Age prediction during development

We analyzed the performance of our model in the development age, therefore we considered the subset of subjects within the 7–20 age range, resulting in 777 subjects with mean age 13 ± 3years, see Fig. 4.

In this case we registered the following results: MAE $= 1.53 \pm 0.02$,RMSE $= 1.94 \pm 0.02$and $\rho = 0.787 \pm 0.006$. Compared to previous results, obtained with the whole dataset, all performance metrics showed significant differences: MAE and RMSE showed an improvement (30%and 24%,respectively) while correlation worsened (12%).

4.4. Sample size and site heterogeneity

We explored the performance accuracy of our model with a varying percentage of training examples to evaluate how sample size affects the model accuracy. The 10-fold cross-validation accuracy of our model was evaluated with an increasing number of subjects, ranging from 10%to 90%.

As expected, we observed a monotone improvement of performance associated with an increasing sample size. Interestingly, we observed two distinct behaviors: with sample size below 40%of all examples, there was a steep descent of MAE; then, the performance continued to improve, but with a lower slope. Results are shown in Fig. 5

To understand how much site heterogeneity affects prediction accuracy, we also computed the median MAE for each site and estimated the related probability density function. In fact, we observed that this distribution is nicely sharp when 70–90% of examples are used. For MAE distribution obtained with 90%of examples, the interquartile range is 0.71 years and 1.23 years for 70%. The distribution width dramatically broadens when using 30%or 10%of examples, in these cases the interquartile range is 1.50 years and 1.96 years, respectively.

4.5. Reliability of network centralities

We evaluated if the model accuracy was affected by our choice of using the nodal strength to characterize the importance of different brain regions. We compared the informative content provided by strength, inverse participation, betweenness and eigenvector centrality. Interestingly, Fig. 6 shows that using other centrality metrics or combining them does not provide any significant improvement.

We performed 100 10-fold cross-validations to compare the model accuracy obtained with strength with the one obtained using the other metrics. A statistical comparison showed that the only significant difference was that found using betweenness; in that case MAE was 3.05. Another interesting aspect is that no significant difference is observed when using all network centralities.

Furthermore, for each network centrality measure we evaluated the inherent feature importance ranking, in order to understand whether, despite the analogous classification performance, centralities exploited different informative contents. We measured the pairwise Spearman's correlation and found on average a 0.8 correlation, thus we concluded no significant differences existed.

4.6. Clinical interpretation

To investigate which features had a strategic role in the age prediction, we calculated variable importance by using the Gedeon method (Gedeon, 1997). This method assesses feature importance by considering the neuronal weights and propagating them through the network (Supplementary Materials Gedeon Method for a mathematical description). Fig. 7 shows a graphic representation of the 12 most important patches for aging (importance greater than 99th quantile of the importance distribution).

We computed the mean score for each feature over different cross-validation rounds; the overall ranking is presented here. The importance of each patch is coded by the patch size, that is linearly related to the patch importance, and by a color scale ranging from blue (lowest importance) to red (highest importance).

Table 4 presents the anatomical regions included in the patches with an importance greater than the 99th quantile. The percentage of voxels that each region occupies in the patch is also reported.

It is interesting to notice that some regions such as extra-nuclear white matter, thalamus, cingulate, putamen and globus pallidus are recurrent in more patches. An exhaustive clinical interpretation of these regions and their strategical role in brain aging is reported in the Discussion.

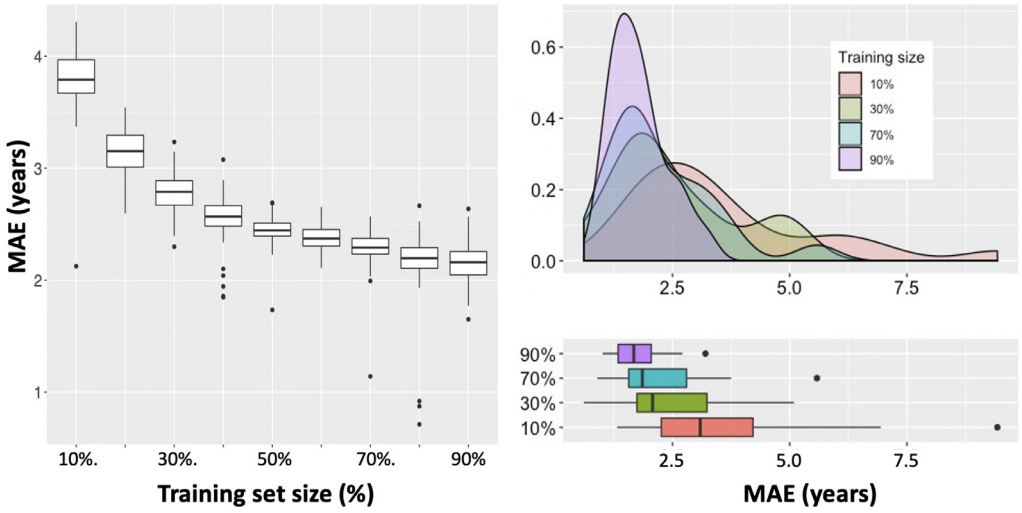

Fig. 5. Left panel: prediction accuracy (MAE) measured by varying the training set size. Right panel: the training set size is varied and the MAE is computed for each site. As the training set increases, MAE variability over different sites decreases.

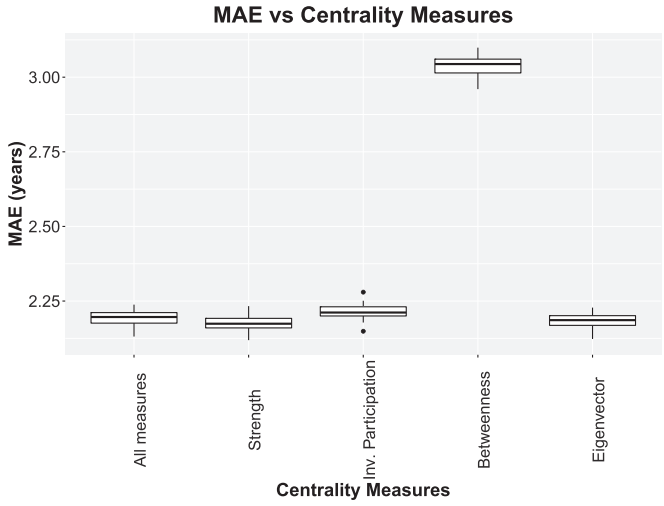

Fig. 6. Despite the use of different centrality measures, the model inherits from almost all metrics the capability to accurately predict brain age. The only significant difference is found when using betweenness, in that case performance accuracy significantly lowers.

5. Discussion

The brain connectivity model, proposed in this work, allows an accurate estimation of brain aging from $T1$MRI scans. The network model remains robust also using different machine learning algorithms. The highest age prediction accuracy (MAE = 2.19) is obtained with deep neural networks and the lowest with random forests. Although these learning algorithms yield significant differences in terms of MAE, on average, they differ by only 0.9 years and analogous small discrepancies are detected with the other metrics. These findings confirm the robustness of our model for brain age prediction and an indirect proof that it yields a good representation of the data under investigation. This is especially true when considering approaches sharing important properties with this study as the use of structural MRI, a similar age range and the focus on ABIDE subjects (Corps and Rekik, 2019; Jiang et al., 2019; Jónsson et al., 2019).

The proposed approach has shown reliable performances with an independent and heterogeneous test set which included ABIDE subjects, sharing acquisition and protocol features similar to the training ones, and subjects from Beijing Normal University. Despite this heterogeneity we observed a limited performance deterioration, especially for what concerns MAE and RMSE: for these metrics results are compatible with those obtained in training within 2 standard deviations. Pearson's cor-

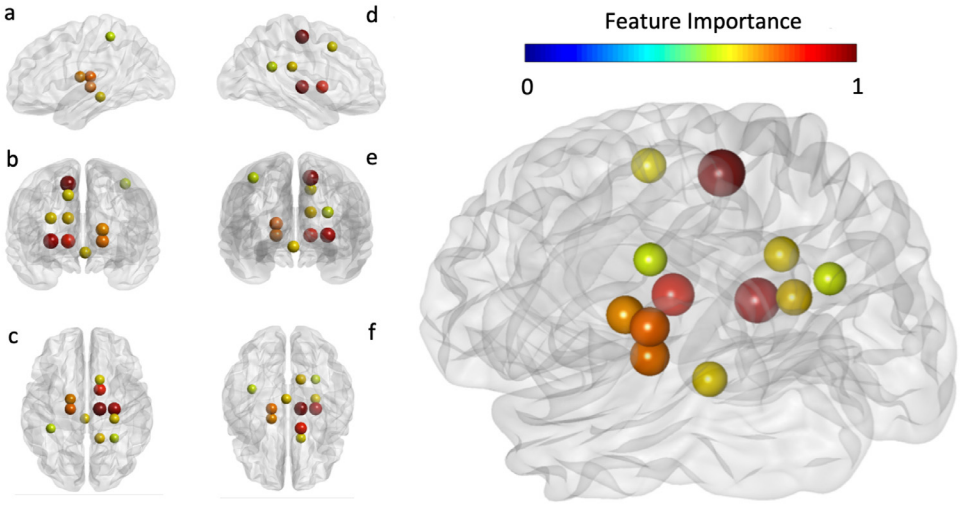

Fig. 7. Glass brain with the most important patches for brain age prediction. Several views are shown: (a) Left Lateral Medial; (b) Anterior; (c) Dorsal; (d) Right Lateral Medial; (e) Posterior; (f) Ventral. Feature importance is represented both by color and size of nodes.

Table 4
Anatomical regions pinpointed by the most important patches along with the corresponding percentage of patch voxels occupied by each region and the mean relative importance associated to each region. It is worth to underline that the anatomical regions with the same importance value are identified by the same patch. BA indicates Brodman area, VLN and LPN indicate Ventral Lateral Nucleus and Lateral Posterior Nucleus, L and R indicate left and right hemispheres, and CSF GM and WM indicate the presence of cerebrospinal fluid, grey matter and white matter in a certain patch.

Anatomical region	Voxel %	Mean relative importance
R Sub-Gyral in Frontal Lobe (WM)	27.7	1.000
R Medial Frontal Gyrus, BA 6 incl. (GM,WM)	48.9	1.000
R Paracentral Lobule (WM)	10.1	1.000
R Sub-lobar Extra-Nuclear (WM)	46	0.946
R Sub-lobar Putamen (GM)	28.5	0.946
R Sub-lobar Lateral Globus Pallidus (GM)	12.9	0.946
R Sub-lobar Extra-Nuclear (WM)	46.9	0.863
R Sub-lobar Putamen (GM)	10.7	0.863
R Sub-lobar Lateral Globus Pallidus (GM)	11.5	0.863
R Sub-lobar Caudate Body (GM)	11.1	0.863
L Sub-lobar Extra-Nuclear (WM)	10.3	0.779
L Sub-lobar Thalamus, VLN & LPN incl. (GM)	56	0.779
L Sub-lobar Extra-Nuclear (WM)	25.9	0.763
L Sub-lobar Thalamus VLN & LPN incl. (GM)	45.2	0.763
L Sub-lobar Extra-Nuclear (WM)	59.3	0.733
L Sub-lobar Thalamus (VLN, GM)	12.2	0.733
R Sub-lobar Extra-Nuclear (WM)	19.7	0.675
R Posterior Cingulate in Limbic Lobe (WM)	43.3	0.675
R Sub-Gyral in Parietal Lobe (WM)	10.2	0.675
R Sub-lobar Extra-Nuclear (WM)	62.47	0.654
L Brainstem (Midbrain)	66	0.651
R Brainstem (Midbrain)	25	0.651
R Medial Frontal Gyrus, BA 32 incl. (GM)	19.5	0.643
R Cingulate Gyrus in Limbic Lobe, BA 24 & 32 incl. (WM)	54.9	0.643
L Inferior Parietal Lobule, BA 40 incl. (GM, WM)	95.6	0.593
R Sub-Gyral in Temporal Lobe (WM)	12.5	0.584
R Sub-Gyral in Parietal Lobe (WM)	26.1	0.584
R Sub-lobar Extra-Nuclear (WM)	56.9	0.584

relation suffers a more evident deterioration, but this is somehow expected as it is well known how sample size affects correlation measures both in terms of stability and accuracy (Bland and Altman, 2011; Schönbrodt and Perugini, 2013). In test, we also observed larger uncertainties about the performance metrics: on one hand, this is a consequence of the accuracy loss suffered by predictions, but on the other hand this effect could also depend on the fact that the age of subjects from the Beijing dataset is given in integers, i.e with a year precision. We also investigated the test performance of ABIDE and Beijing subjects, separately. We observed that ABIDE test predictions were compatible with the training ones, except for correlation; although Beijing predictions suffered a more significant loss, even in this case we observed a substantial agreement with cross-validation estimates, suggesting that the model was able to generalize to novel unseen data.

The model accuracy (MAE = 1.53) and stability was also proved when considering only developmental subjects (7–20 years). Several age prediction models ranging from early childhood to young adulthood have been developed so far (Ball et al., 2017; Brown et al., 2012; Cao et al., 2015; Dosenbach et al., 2010; Erus et al., 2015; Khundrakpam et al., 2015; Wang et al., 2014), with accuracies for brain age predictions ranging in from $\rho = 0.43$to $\rho = 0.96$,and MAEs from 1.0 to 1.9 years. In general, the model accuracy compares well with the state-of-the-art (Franke et al., 2017).

Comparing results about ranges 7–20 years and 7–40 years, MAE and RMSE improved compared to overall results, while Pearson's correlation showed a worsening. This effect can be explained on one hand taking into account the specificity of the ABIDE I dataset: the age distribution is clearly unbalanced, thus considering a restricted age range allows a more effective learning and an improvement of MAE and RMSE; for what concerns correlation, again we should note the effect of sample of size on this metric.

Data heterogeneity, cross-validation framework, sample size and age range are determinant features when considering age prediction. For example, a BrainAGE study (Franke et al., 2012) carried out in leave-one-out on 394 with data collected from six different size and patients with a sharper age range (with average 10.7 ± 3.9years) led to a slightly better performance of MAE = 1.1years and correlation $\rho = 0.93$. An analogous study was carried out on wider age ranges Franke et al. (2010). This study employed scans from three different scanners and 550 individuals aged 19–86 years and an independent test, collected on a fourth scanner, from 108 subjects, aged 20–59 years. In this case, the authors reported $\rho = 0.92$and MAE = 5years; although using analogous prediction models, results can severely be affected by previously mentioned aspects.

The interest to age prediction with deep learning methods has recently grown, as testified for example by the international challenge Predictive Analytics Competition 2019[6], held in 2019. The winning algorithm (Peng et al., 2019), using lightweight deep neural networks, reported a 2.90 MAE years on a testing cohort of 2638 subjects. Recently, a Convolutional Neural Network was employed to predict brain age from a large dataset of healthy subjects aged 18–90 years (Cole et al., 2018). This study reported a MAE of 4.65 years for MRI raw data, thus demonstrating the effectiveness and reliability of deep learning approaches. In Amoroso et al. (2019) we also implemented a pipeline for brain age prediction exploiting deep learning. However, age predictions were obtained on a smaller cohort of 484 individuals from 5 publicly available sources with a roughly uniform age distribution in the range 7–80 years. The present analysis has significantly improved those results. Besides the

[6] https://web.archive.org/web/20200214101600/ https://www.photon-ai.com/pac2019 .

differences in terms of performance and data, it is also remarkable that in the present study a different and simpler network model was adopted.

Neuroimaging processing pipelines include several different options and packages, thus in many cases the computational burden can be difficult to afford and requires dedicated ICT resources. Furthermore, in the case of pediatric imaging, particular techniques as special masking or dedicated templates for spatial normalization are needed. On the contrary, our approach minimizes image processing techniques to the basic aspects of intensity and spatial normalization. Besides, as each technique adopts its specific assumptions, their use yields the need to consider additional confounds.

Investigating the effect of sample size on the performance, we found that accuracy experiences a continuous deterioration as the training sample size reduces. This trend can be accurately fitted by a power law. Although this behavior has been already observed in homogeneous datasets (He et al., 2020; Schulz et al., 2019), we would not exclude here a possible relation with data heterogeneity. When less than 50%of training data is considered, the diversity of sites, protocols and the skewness of age distribution could impair the learning (Castrillon et al., 2014; Nielsen et al., 2013).

However, our results confirm that this performance loss is mitigated by increasing size of training; in fact, it is known that a key parameter determining age prediction accuracy is the training sample size (Franke et al., 2010).

The proposed network model exploits nodal centrality to assess how different brain regions affect aging. We demonstrated that the informative content of the proposed approach does not depend on the specific centrality measure adopted. In fact, all centrality measures perform equally in terms of model accuracy; the only exception is betweenness, but this is somehow reasonable. Strength, inverse participation and eigenvector centrality are centrality measures that, with a slightly different nuance, capture the direct effect of a node onto its neighbors; betweenness is conceptually different as it is a measure of indirect effects (Freeman, 1978; Friedkin, 1991). Accordingly, direct measures must be preferred; furthermore, direct measures are easier to interpret and this is an advantage, especially for clinical purposes.

Our results show that sub-lobar extra-nuclear white matter and thalamus, identified by the most important patches for a total of 5186 voxels and 1702 voxels, respectively, play a central role in aging. Extranuclear white matter has been widely reported as a region involved in the aging process and responsible for the compensatory ventricular enlargement due to the brain volume decrease associated with age (Whitacre, 2008). The Thalamus is a strategical brain region supporting cognitive functions known to decline in normal aging such as memory, attention and information processing. Multimodal brain imaging has revealed age-related thalamic changes over the adult lifespan. In particular, integrity of the thalamic nuclei were found to decline with advancing age and their size was found to correlate with the ability to perform cognitive processes involving attention and memory (Fama and Sullivan, 2015; Tullo et al., 2019). Several studies observed brain changes related to age in putamen, caudate, medial frontal gyrus, cingulate, brainstem and sub-gyral regions, therefore fully in agreement with our findings (Abe et al., 2008; Amoroso et al., 2019; Cortés et al., 2015; Zhao et al., 2019),Lombardi et al.. Age-related gray matter atrophy in cingulate gyrus has always been a debated topic and literature studies have been conflicting Terribilli et al. (2011). However, PET and FDG-PET studies have shown metabolic age-related changes in Brodman area 24 and 32 of the cingulate gyrus and in Brodman area 6 of the medial frontal gyrus, in line with our results Charney et al. (2013).

6. Conclusions

In this work we present a thorough framework for age prediction based on a robust complex network approach yielding a structural connectivity description. Age prediction based on our network model is highly accurate and the findings are confirmed even when considering subjects in developmental age. Network centralities are suitable metrics to characterize aging patterns, in particular, the strength of nodal connections best captures the brain changes over time. Finally, the model proposed is easy to interpret and yields an importance ranking of brain regions affecting age prediction accuracy. The model is somewhat affected by data heterogeneity, in particular due to multi-site variability; while sample size increases the model accuracy, data heterogeneity impairs the learning phase. Although prediction remains accurate, future studies addressing data harmonization techniques and including them in the framework could further improve the accuracy and reliability.

Data and code availability

ABIDE data, neuroimaging software and connectivity/learning software are publicly available or based on publicly available languages; further details about the analyses can be requested by contacting the authors.

Supplementary material

Supplementary material associated with this article can be found, in the online version, at 10.1016/j.neuroimage.2020.117458

References

Abe, O., Yamasue, H., Aoki, S., Suga, M., Yamada, H., Kasai, K., Masutani, Y., Kato, N., Kato, N., Ohtomo, K., 2008. Aging in the CNS: comparison of gray/white matter volume and diffusion tensor data. Neurobiol. Aging 29 (1), 102–116.

Abellaneda-Pérez, K., Vaqué-Alcázar, L., Vidal-Piñeiro, D., Jannati, A., Solana, E., Bargalló, N., Santarnecchi, E., Pascual-Leone, A., Bartrés-Faz, D., 2019. Age-related differences in default-mode network connectivity in response to intermittent theta-burst stimulation and its relationships with maintained cognition and brain integrity in healthy aging. NeuroImage 188, 794–806.

Amoroso, N., La Rocca, M., Bellantuono, L., Diacono, D., Fanizzi, A., Lella, E., Lombardi, A., Maggipinto, T., Monaco, A., Tangaro, S., et al., 2019. Deep learning and multiplex networks for accurate modeling of brain age. Front. Aging Neurosci. 11, 115.

Amoroso, N., La Rocca, M., Bruno, S., Maggipinto, T., Monaco, A., Bellotti, R., Tangaro, S., 2018. Multiplex networks for early diagnosis of Alzheimer's disease. Front. Aging Neurosci. 10, 365.

Amoroso, N., La Rocca, M., Monaco, A., Bellotti, R., Tangaro, S., 2018. Complex networks reveal early MRI markers of Parkinsons disease. Med. Image Anal. 48, 12–24.

Ashburner, J., 2007. A fast diffeomorphic image registration algorithm. Neuroimage 38 (1), 95–113.

Avants, B.B., Tustison, N.J., Song, G., Cook, P.A., Klein, A., Gee, J.C., 2011. A reproducible evaluation of ANTs similarity metric performance in brain image registration. Neuroimage 54 (3), 2033–2044.

Aycheh, H.M., Seong, J.-K., Shin, J.-H., Na, D.L., Kang, B., Seo, S.W., Sohn, K.-A., 2018. Biological brain age prediction using cortical thickness data: a large scale cohort study. Front. Aging Neurosci. 10, 252.

Bagarinao, E., Watanabe, H., Maesawa, S., Mori, D., Hara, K., Kawabata, K., Yoneyama, N., Ohdake, R., Imai, K., Masuda, M., et al., 2019. Reorganization of brain networks and its association with general cognitive performance over the adult lifespan. Sci. Rep. 9 (1), 1–15.

Ball, G., Adamson, C., Beare, R., Seal, M.L., 2017. Modelling neuroanatomical variation during childhood and adolescence with neighbourhood-preserving embedding. Sci. Rep. 7 (1), 112.

Benou, A., Veksler, R., Friedman, A., Raviv, T.R., 2017. Ensemble of expert deep neural networks for spatio-temporal denoising of contrast-enhanced MRI sequences. Med. Image Anal. 42, 145–159.

Betzel, R.F., Bassett, D.S., 2017. Multi-scale brain networks. Neuroimage 160, 73–83.

Bland, J.M., Altman, D.G., 2011. Correlation in restricted ranges of data. BMJ 342, d556.

Brown, T.T., Kuperman, J.M., Chung, Y., Erhart, M., McCabe, C., Hagler Jr., D.J., Venkatraman, V.K., Akshoomoff, N., Amaral, D.G., Bloss, C.S., Casey, B.J., Chang, L., Ernst, T.M., Frazier, J.A., Gruen, J.R., Kaufmann, W.E., Kenet, T., Kennedy, D.N., Dale, A.M., 2012. Neuroanatomical assessment of biological maturity. Curr. Biol. 22, 1693–1698.

Bullmore, E., Sporns, O., 2009. Complex brain networks: graph theoretical analysis of structural and functional systems. Nat. Rev. Neurosci. 10 (3), 186–198.

Cannistraci, C.V., Alanis-Lobato, G., Ravasi, T., 2013. From link-prediction in brain connectomes and protein interactomes to the local-community-paradigm in complex networks. Sci. Rep. 3 (1), 1–14.

Cao, B., Mwangi, B., Hasan, K.M., Selvaraj, S., Zeni, C.P., Zunta-Soares, G.B., Soares, J.C., 2015. Development and validation of a brain maturation index using longitudinal neuroanatomical scans. Neuroimage 117, 311–318.

Castrillon, J.G., Ahmadi, A., Navab, N., Richiardi, J., 2014. Learning with multi-site FMRI graph data. In: 2014 48th Asilomar Conference on Signals, Systems and Computers. IEEE, pp. 608–612.

Charney, D.S., Buxbaum, J.D., Sklar, P., Nestler, E.J., 2013. Neurobiology of Mental Illness. Oxford University Press.
Cole, J.H., Franke, K., 2017. Predicting age using neuroimaging: innovative brain ageing biomarkers. Trends Neurosci. 40 (12), 681–690.
Cole, J.H., Marioni, R.E., Harris, S.E., Deary, I.J., 2019. Brain age and other bodily ages: implications for neuropsychiatry. Mol. Psychiatry 24 (2), 266–281.
Cole, J.H., Poudel, R.P., Tsagkrasoulis, D., Caan, M.W., Steves, C., Spector, T.D., Montana, G., 2017. Predicting brain age with deep learning from raw imaging data results in a reliable and heritable biomarker. NeuroImage 163, 115–124.
Cole, J.H., Ritchie, S.J., Bastin, M.E., Hernández, M.V., Maniega, S.M., Royle, N., Corley, J., Pattie, A., Harris, S.E., Zhang, Q., et al., 2018. Brain age predicts mortality. Mol. Psychiatry 23 (5), 1385–1392.
Corps, J., Rekik, I., 2019. Morphological brain age prediction using multi-view brain networks derived from cortical morphology in healthy and disordered participants. Sci. Rep. 9 (1), 110.
Cortés, J.M., Marinazzo, D., Muñoz, M.A., 2015. Information-based methods for neuroimaging: analyzing structure, function and dynamics. Front. Media SA.
Damoiseaux, J.S., 2017. Effects of aging on functional and structural brain connectivity. Neuroimage 160, 32–40.
Di Martino, A., Yan, C.-G., Li, Q., Denio, E., Castellanos, F.X., Alaerts, K., Anderson, J.S., Assaf, M., Bookheimer, S.Y., Dapretto, M., et al., 2014. The autism brain imaging data exchange: towards a large-scale evaluation of the intrinsic brain architecture in autism. Mol. Psychiatry 19 (6), 659–667.
Dosenbach, N.U.F., Nardos, B., Cohen, A.L., Fair, D.A., Power, J.D., Church, J.A., Nelson, S.M., Wig, G.S., Vogel, A.C., Lessov-Schlaggar, C.N., Barnes, K.A., Dubis, J.W., Feczko, E., Coalson, R.S., Pruett Jr., J.R., Barch, D.M., Petersen, S.E., Schlaggar, B.L., 2010. Prediction of individual brain maturity using fMRI. Science 329, 1358–1361.
Durstewitz, D., Koppe, G., Meyer-Lindenberg, A., 2019. Deep neural networks in psychiatry. Mol. Psychiatry 24 (11), 1583–1598.
Erus, G., Battapady, H., Satterthwaite, T.D., Hakonarson, H., Gur, R.E., Davatzikos, C., Gur, R.C., 2015. Imaging patterns of brain development and their relationship to cognition. Cereb. Cortex 25 (6), 1676–1684.
Fama, R., Sullivan, E.V., 2015. Thalamic structures and associated cognitive functions: relations with age and aging. Neurosci. Biobehav. Rev. 54, 29–37.
Feng, X., Lipton, Z.C., Yang, J., Small, S.A., Provenzano, F.A., Initiative, A.D.N., Initiative, F.L.D.N., et al., 2020. Estimating brain age based on a uniform healthy population with deep learning and structural MRI. Neurobiol. Aging.
Fjell, A.M., Walhovd, K.B., 2010. Structural brain changes in aging: courses, causes and cognitive consequences. Rev. Neurosci. 21 (3), 187–222.
Franke, K., Bublak, P., Hoyer, D., Billiet, T., Gaser, C., Witte, O., Schwab, M., 2017. In vivo biomarkers of structural and functional brain development and aging in humans. Neurosci. Biobehav. Rev..
Franke, K., Gaser, C., 2019. Ten years of BrainAGE as a neuroimaging biomarker of brain aging: What insights have we gained? Frontiers in neurology 10, 789.
Franke, K., Luders, E., May, A., Wilke, M., Gaser, C., 2012. Brain maturation: predicting individual BrainAGE in children and adolescents using structural MRI. Neuroimage 63, 1305–1312.
Franke, K., Ziegler, G., Klöppel, S., Gaser, C., Initiative, A.D.N., et al., 2010. Estimating the age of healthy subjects from t1-weighted MRI scans using kernel methods: exploring the influence of various parameters. Neuroimage 50 (3), 883–892.
Freeman, L.C., 1978. Centrality in social networks conceptual clarification. Soc. Netw. 1 (3), 215–239.
Friedkin, N.E., 1991. Theoretical foundations for centrality measures. Am. J. Sociol. 96 (6), 1478–1504.
Gedeon, T.D., 1997. Data mining of inputs: analysing magnitude and functional measures. Int. J. Neural Syst. 8 (02), 209218.
He, T., Kong, R., Holmes, A.J., Nguyen, M., Sabuncu, M.R., Eickhoff, S.B., Bzdok, D., Feng, J., Yeo, B.T., 2020. Deep neural networks and kernel regression achieve comparable accuracies for functional connectivity prediction of behavior and demographics. NeuroImage 206, 116276.
Ho, Y.-C., Pepyne, D.L., 2002. Simple explanation of the no-free-lunch theorem and its implications. J. Optim. Theory Appl. 115 (3), 549–570.
Hoerl, A., 1986. Kennard, r. w. 1970. Ridge regression: Biased esti.
Jenkinson, M., Pechaud, M., Smith, S., et al., 2005. BET2: MR-based estimation of brain, skull and scalp surfaces. In: Eleventh Annual Meeting of the Organization for Human Brain Mapping, 17. Toronto., p. 167.
Jiang, H., Lu, N., Chen, K., Yao, L., Li, K., Zhang, J., Guo, X., 2019. Predicting brain age of healthy adults based on structural MRI parcellation using convolutional neural networks. Front. Neurol. 10.
Jónsson, B.A., Bjornsdottir, G., Thorgeirsson, T., Ellingsen, L.M., Walters, G.B., Gudbjartsson, D., Stefansson, H., Stefansson, K., Ulfarsson, M., 2019. Brain age prediction using deep learning uncovers associated sequence variants. Nat. Commun. 10 (1), 110.
Khundrakpam, B.S., Tohka, J., Evans, A.C., Brain Development Cooperative Group, 2015. Prediction of brain maturity based on cortical thickness at different spatial resolutions. Neuroimage 111, 350–359.
Konukoglu, E., Glocker, B., Zikic, D., Criminisi, A., 2013. Neighbourhood approximation using randomized forests. Med. Image Anal. 17 (7), 790–804.
La Rocca, M., Amoroso, N., Monaco, A., Bellotti, R., Tangaro, S., Initiative, A.D.N., et al., 2018. A novel approach to brain connectivity reveals early structural changes in Alzheimers disease. Physiol. Meas. 39 (7), 074005.
Leibig, C., Allken, V., Ayhan, M.S., Berens, P., Wahl, S., 2017. Leveraging uncertainty information from deep neural networks for disease detection. Sci. Rep. 7 (1), 1–14.
Liaw, A., Wiener, M., et al., 2002. Classification and regression by randomforest. R News 2 (3), 18–22.
Lombardi, A., Amoroso, N., Diacono, D., Monaco, A., Tangaro, S., Bellotti, R., Extensive evaluation of morphological statistical harmonization for brain age predictio. Brain Sci..
Lombardi, A., Guaragnella, C., Amoroso, N., Monaco, A., Fazio, L., Taurisano, P., Pergola, G., Blasi, G., Bertolino, A., Bellotti, R., et al., 2019. Modelling cognitive loads in schizophrenia by means of new functional dynamic indexes. NeuroImage 195, 150–164.
Madan, C.R., Kensinger, E.A., 2018. Predicting age from cortical structure across the lifespan. Eur. J. Neurosci. 47 (5), 399–416.
Mukaka, M.M., 2012. A guide to appropriate use of correlation coefficient in medical research. Malawi Med. J. 24 (3), 69–71.
Nielsen, J.A., Zielinski, B.A., Fletcher, P.T., Alexander, A.L., Lange, N., Bigler, E.D., Lainhart, J.E., Anderson, J.S., 2013. Multisite functional connectivity MRI classification of autism: ABIDE results. Front. Hum. Neurosci. 7, 599.
Peng, H., Gong, W., Beckmann, C. F., Vedaldi, A., Smith, S. M., 2019. Accurate brain age prediction with lightweight deep neural networks. BioRxiv.
Putin, E., Mamoshina, P., Aliper, A., Korzinkin, M., Moskalev, A., Kolosov, A., Ostrovskiy, A., Cantor, C., Vijg, J., Zhavoronkov, A., 2016. Deep biomarkers of human aging: application of deep neural networks to biomarker development. Aging 8 (5), 1021.
Qi, T., Schaadt, G., Cafiero, R., Brauer, J., Skeide, M.A., Friederici, A.D., 2019. The emergence of long-range language network structural covariance and language abilities. NeuroImage 191, 36–48.
Roriz-Filho, J.S., Sá-Roriz, T.M., Rosset, I., Camozzato, A.L., Santos, A.C., Chaves, M.L., Moriguti, J.C., Roriz-Cruz, M., 2009. (pre) diabetes, brain aging, and cognition. Biochim. Biophys. Acta (BBA)-Mol. Basis Dis. 1792 (5), 432–443.
Sabuncu, M.R., Van Leemput, K., 2012. The relevance voxel machine (RVoxM): a self-tuning Bayesian model for informative image-based prediction. IEEE Trans. Med. Imaging 31 (12), 2290–2306.
Schnack, H.G., Van Haren, N.E., Nieuwenhuis, M., Hulshoff Pol, H.E., Cahn, W., Kahn, R.S., 2016. Accelerated brain aging in schizophrenia: a longitudinal pattern recognition study. Am. J. Psychiatry 173 (6), 607–616.
Schönbrodt, F.D., Perugini, M., 2013. At what sample size do correlations stabilize? J. Res. Pers. 47 (5), 609–612.
Schulz, M.-A., Yeo, T., Vogelstein, J., Mourao-Miranada, J., Kather, J., Kording, K., Richards, B. A., Bzdok, D., 2019. Deep learning for brains?: Different linear and nonlinear scaling in UK Biobank brain images vs. machine-learning datasets. BioRxiv, 757054.
Smola, A., Schölkopf, B., 2004. A tutorial on support vector regression. Stat. Comput. 14, 199222.
Spreng, R.N., Stevens, W.D., Viviano, J.D., Schacter, D.L., 2016. Attenuated anticorrelation between the default and dorsal attention networks with aging: evidence from task and rest. Neurobiol. Aging 45, 149–160.
Terribilli, D., Schaufelberger, M.S., Duran, F.L., Zanetti, M.V., Curiati, P.K., Menezes, P.R., Scazufca, M., Amaro Jr, E., Leite, C.C., Busatto, G.F., 2011. Age-related gray matter volume changes in the brain during non-elderly adulthood. Neurobiol. Aging 32 (2), 354–368.
Tibshirani, R., 1996. Regression shrinkage and selection via the lasso. J. R. Stat. Soc. 58 (1), 267288.
Tipping, M.E., 2000. The relevance vector machine. In: Advances in Neural Information Processing Systems, p. 652658.
Tullo, S., Patel, R., Devenyi, G.A., Salaciak, A., Bedford, S.A., Farzin, S., Wlodarski, N., Tardif, C.L., Group, P.-A.R., Breitner, J.C., et al., 2019. Mr-based age-related effects on the striatum, globus pallidus, and thalamus in healthy individuals across the adult lifespan. Hum. Brain Map. 40 (18), 5269–5288.
Tustison, N.J., Avants, B.B., Cook, P.A., Zheng, Y., Egan, A., Yushkevich, P.A., Gee, J.C., 2010. N4itk: improved n3 bias correction. IEEE Trans. Med. Imaging 29 (6), 1310–1320.
Wang, J., Li, W., Miao, W., Dai, D., Hua, J., He, H., 2014. Age estimation using cortical surface pattern combining thickness with curvatures. Med. Biol. Eng. Comput. 52, 331–341.
Whitacre, D.M., 2008. Reviews of Environmental Contamination and Toxicology, 202. Springer.
Wu, Z., Peng, Y., Selvaraj, S., Schulz, P.E., Zhang, Y., 2020. Development of brain structural networks over age 8: a preliminary study based on diffusion weighted imaging. Front. Aging Neurosci. 12, 61.
Zahr, N.M., 2018. The aging brain with HIV infection: effects of alcoholism or hepatitis C comorbidity. Front. Aging Neurosci. 10, 56.
Zhao, Y., Klein, A., Castellanos, F.X., Milham, M.P., 2019. Brain age prediction: cortical and subcortical shape covariation in the developing human brain. NeuroImage 202, 116149.
Zhou, C., Zemanová, L., Zamora, G., Hilgetag, C.C., Kurths, J., 2006. Hierarchical organization unveiled by functional connectivity in complex brain networks. Phys. Rev. Lett. 97 (23), 238103.
Zou, H., Hastie, T., 2005. Regularization and variable selection via the elastic net. J. R. Stat. Soc. 67 (2), 301–320.